Lipid Microdomain Formation: Characterization by Infrared Spectroscopy and Ultrasonic Velocimetry

Zachary D. Schultz and Ira W. Levin
Laboratory of Chemical Physics, National Institute of Diabetes and Digestive and Kidney Diseases, National Institutes of Health, Bethesda, Maryland 20892

ABSTRACT We demonstrate the use of vibrational infrared spectroscopy applied to characterize lipid microdomain sizes derived from a model raft-like system consisting of nonhydroxy galactocerebroside, cholesterol, and dipalmitoylphosphatidylcholine components. The resulting spectroscopic correlation field components of the lipid acyl chain CH_2 methylene deformation modes, observed when lipid multilamellar assemblies are rapidly frozen from the liquid crystalline state to the gel phase, indicate the existence of lipid microdomains on a scale of several nanometers. The addition of cholesterol disrupts the glycosphingolipid selectively but perturbs the di-saturated chain phospholipid matrix. Complementary acoustic velocimetry measurements indicate that the microdomain formation decreases the total volume adiabatic compressibilities of the multilamellar vesicle assemblies. The addition of cholesterol, however, disrupts the galactocerebroside domains, resulting in a slight increase in the lipid assemblies' total adiabatic compressibility. The combination of these two physical approaches offers new insight into microdomain formation and their properties in model bilayer systems.

INTRODUCTION

The existence of microdomains in cell membranes and their role in cellular processes, such as cellular adhesion, intracellular trafficking, and cell recognition, continues to be an area of intense research (1–4). Although a variety of physical and chemical interactions gives rise to the heterogeneity of the bilayer membrane and the formation of discrete molecular clusters, essential features of these microdomain complexes remain poorly understood. The observations that certain membranes enriched in glycosphingolipids and cholesterol exhibit aggregates that are poorly soluble in detergents at low temperatures led to the hypothesis that the membrane contained specific lipid clusters, commonly termed ''rafts'' (5–10). Efforts to detect and to characterize these lipid raft domains in intact membranes led to the consideration that numerous microdomains, in addition to raft-type structures, exist in biological membranes, thus emphasizing the ''mosaicism'' of the Singer-Nicholson model to better reflect the current understanding of membrane bilayer architecture (3). The inherent complexity, however, of intact cellular membranes increases the difficulties inherent in the detection and characterization of general, microdomain clusters within these systems (11).

Despite the implicit complexity of in vivo systems, various model bilayer membrane systems provide a wealth of information regarding the lipid-lipid and lipid-protein interactions governing the properties of microdomain clusters (11,12). Although model systems clearly indicate domain formation, the relationship of model systems to the size and organization of microdomains in intact membranes remains uncertain (11). Indeed, the language used to describe lipid assemblies has grown to include broad terms, such as ''nanoclusters'', ''shells'', ''domains'', and ''rafts'', to reflect the differences in their size and composition. Although phase separation and energy minimization arguments support the formation of large domains, which have been experimentally observed at equilibrium (13), an alternative hypothesis to equilibrium lipid domains in intact membranes is the possibility that these aggregates reflect a reorganization of nonequilibrium systems in response to various stimuli (4).

Biomembranes, thus, present a unique experimental challenge for measuring bilayer clusters on submicrometer scales with a minimum perturbation applied to the system. Fluorescence spectroscopic and imaging methods have provided significant information regarding lipid microdomain behavior (14,15). For example, fluorescence resonance energy transfer (FRET) detects the interaction of donor and acceptor probes and is sensitive to distances of a few nanometers, depending on the Forster radii of the probes. Indeed, FRET has been reported to support the existence of liquid-ordered and liquid-disordered heterogeneous domains smaller than 20 nm in intact cell membranes (16). An increasing number of reports suggests, however, that fluorescent labels may result in undesirable interactions necessitating complementary techniques, independent of the fluorescent tags, to confirm microdomain formation (17–19). Although atomic force microscopy (AFM) has imaged model system domains of varying sizes (15), the technique suffers from an uncertainty regarding the influence of substrates (20), as well as possible tip-induced effects, which may drag multiple small domains together (21). Mass spectrometry represents a label-free technique that demonstrates capabilities in chemical imaging with a spatial resolution of ~100 nm (22). Although mass spectrometry used in conjunction with supported bilayer membranes also suffers from substrate effects, probes that provide new nanoscale in-

Submitted August 15, 2007, and accepted for publication December 11, 2007.

Address reprint requests to Ira W. Levin, E-mail: iwl@helix.nih.gov.

Editor: Michael Edidin.

0006-3495/08/04/3104/11 $2.00

doi: 10.1529/biophysj.107.119735

formation should prove critical in elucidating the details and functions of these bilayer lipid aggregates.

Although significant effort has gone into the detection and characterization of lipid microdomains, clarification of the roles of these clusters in modulating the behavior of cellular membrane activities is equally important. To understand the interplay between lipid aggregation and the mechanical properties of the bilayer, we combined in this study vibrational infrared spectroscopy and ultrasonic velocimetry to clarify underlying bilayer interactions. For example, channel formation by gramacidin is enhanced by tailoring the mechanical properties of the bilayer either by modulating the bilayer thickness with varying length lipids or by adding cholesterol or other molecules that presumably make the bilayer more amenable to the formation of the membrane-spanning dimer (23–25). Additionally, the increasing importance of microdomain structures in intact membranes suggests that integral membrane protein regulation is a function of the microdomain environment surrounding the protein. It is also well known that reconstitution of membrane proteins in bilayer assemblies is dependent on the lipid composition of the model membrane, although whether this represents a specific chemical interaction or a more general mechanical effect remains to be determined (26).

Infrared spectroscopic techniques have long provided a wealth of chemical information regarding lipids and biomembranes (27,28); these approaches now also offer potentially useful experimental routes for determining the size of small lipid microdomains, such as rafts. Additionally, infrared spectroscopy is advantageous since no exogenous labels are introduced, thus eliminating the possibility of artifactual interactions; furthermore, molecular species can be distinguished through the incorporation of appropriately substituted isotopic components. Compared to other techniques, the isotopic label in vibrational spectroscopy provides a unique spectral signal without changing the chemical interactions of the labeled molecule. Based on methods originally developed for long chain alkanes (29), the vibrational correlation field splitting parameters that occur in the lipid acyl chain methylene deformation modes permit an estimate of the number of hydrocarbon, alkane chains clustering together in small aggregates of $<$100–150 chains.

As we will note below, the splitting occurs in CH_2 methylene deformation mode as a consequence of interchain vibrational coupling between methylene-coupled oscillators packed in a lipid orthorhombic subcell. The magnitude of the splitting between the two deformation mode correlation field components is proportional to the number of interacting chains. Snyder and Mendelsohn demonstrated that domains consisting of different length saturated lipids exhibited temperature-dependent segregation properties from single molecules to microaggregates of up to 100 molecules (30,31). The kinetics of domain formation was reported in a ceramide/fatty acid/cholesterol stratum corneum model system using this approach (32). Clearly, there is further potential for adapting this general methodology to other biophysical systems.

The systems characterized by infrared spectroscopy can be further probed by acoustic velocimetry for measuring various intensive properties of lipid assemblies. Phase transitions have been reported using acoustic spectroscopy, in agreement with conventional calorimetry (33). The ability of the lipid matrix to modulate protein behavior reflects the lipids' ability to compensate for changes in protein conformation, as, for example, in the case of rhodopsin adjusting to the volume change accompanying the photoisomerization of the retinal chromophore (34–36) or for gramacidin in thinning the bilayer to minimize hydrophobic interactions as the peptide dimer spans the membrane. These changes reflect elastic properties of lipids that can also be characterized by the total compressibility of the system. From accurate measurements of ultrasonic velocity and sample densities, the adiabatic compressibility of the lipid bilayer matrix can be determined (37). This analysis has been demonstrated for lipids and lipid protein complexes, such as blood lipoproteins and polyunsaturated lipid-cholesterol aggregates (38,39) as well as compressibility changes accompanying protein-folding events (40,41). Indeed, heating nisin encapsulated in liposomes led to increased compressibility and loss of structure (42).

Here, we apply vibrational infrared spectroscopy to estimate lipid microdomain sizes at the nanometer level in a model ternary bilayer assembly composed of nonhydroxy galactocerebroside (GalCer)/cholesterol (Chol)/dipalmitoylphosphatidylcholine (DPPC) as a model for a lipid raft system. The spectroscopic technique is combined with adiabatic compressibility measurements obtained from ultrasonic velocimetry for assessing microcluster effects on overall bilayer properties. In contrast to previous domain characterization by infrared spectroscopy, rapid freezing of the sample is used to capture, as a snapshot, the nonequilibrium distribution of lipids present in the liquid crystalline phase and to present the bilayers in a more amenable state for study, namely, the gel phase, where diffusion slows by $\sim$2 orders of magnitude. The low temperature gel phase is annealed to form orthorhombic subcell lipid chain structures from which vibrational selection rules allow band splittings of the lipid chain methylene deformation modes to be observed; these band frequencies are then related to the number of chains comprising the lipid microdomain. In particular, the interactions between nonhydroxy GalCer, Chol, and DPPC are explored in terms of aggregate size, preferred associations, and resulting compressibility properties.

MATERIALS AND METHODS

Materials

The reagents used in this work were either analytical or high performance liquid chromatography grade. Nonhydroxy GalCer with both a protonated and perdueterated octadecanoic acid side chain (GalCer and GalCer-d_{35}) were purchased from Matreya (Pleasant Gap, PA) and used without further purifi-

cation. Cholesterol (≥99%) was purchased from Sigma-Aldrich (St. Louis, MO). 1,2-dimyristoyl-*sn*-glycero-3-phoshocholine (DMPC), 1,2-dipalmitoyl-*sn*-glycero-3-phoshocholine (DPPC), 1,2-dipalmitoyl-d_{62}-*sn*-glycero-3-phoshocholine (DPPC-d_{62}), 1,2-distearoyl-*sn*-glycero-3-phoshocholine (DSPC), and 1,2-distearoyl-d_{70}-*sn*-glycero-3-phoshocholine (DSPC-d_{70}) were purchased from Avanti Polar Lipids (Alabaster, AL). Ultrapure water (KD Medical, Columbia, MD) was used for all samples. The structures of the lipids used in the model raft, GalCer, DPPC, and Chol, are illustrated in Fig. 1.

Sample preparation

Multilamellar binary GalCer/DPPC and ternary GalCer/Chol/DPPC mixtures were prepared by combining the appropriate amounts measured volumetrically from stock solutions of lipids in chloroform. The final molar ratios of GalCer/DPPC and GalCer/Chol/DPPC were 1:1 and 1:0.33:1, respectively. Solvent was evaporated under a stream of N_2 gas and then left under vacuum overnight. The mixtures were dispersed in H_2O. To ensure complete hydration and mixing, the dispersed mixtures were heated above the GalCer T_m to ~95°C, vortexed for 30 s, and then rapidly (within 1–2 min) cooled below the gel to liquid crystalline transition temperature (typically to 0°C). This heating-cooling cycle was repeated at least five times.

For infrared spectroscopic measurements, the aqueous dispersions were deposited between ZnSe windows whose edges were sealed with Teflon tape. Rapid cooling captures the lipids in a spatial distribution reflective of that occurring in the liquid crystalline phase before being immobilized in the gel phase. Once in the gel phase, the lipid acyl chains were annealed at a temperature well below T_m (typically to −25°C) in a cryostat assembly before cooling the sample to −120°C for measuring the infrared absorption spectrum. This annealing procedure, well below the gel to liquid crystalline phase transition, allows the reorganization of the acyl chains into the desired orthorhombic or distorted orthorhombic subcell configuration with no further lipid diffusion.

Ultrasonic measurements required further dilution of the dispersion to ~1% (wt %) lipid in H_2O. The diluted samples were subjected to an additional 10 heating-cooling cycles and degassed under reduced pressure before density and ultrasonic velocimetry measurements.

Infrared spectroscopy

Infrared spectroscopy was performed using a Bomem DA 3.02 Fourier transform spectrometer equipped with a HgCdTe liquid N_2 cooled detector and a KBr beam splitter (ABB Bomem, Quebec, Canada). Spectra were collected at 0.5 cm^{-1} resolution. Typically, 64 interferograms were collected, coadded, and Fourier transformed. Hamming apodization was used for the Fourier transform. The spectrometer was operated under a continuous dry N_2 gas purge to remove interference from atmospheric CO_2 and H_2O vapor. The reference spectrum was collected under identical experimental condition using blank ZnSe windows. Temperature control was achieved using a N_2 purged liquid N_2 cooled cryostat (Cryo Industries, Manchester, NH). Spectra were processed using Grams/AI v.7.02 software (Thermo Galactic, Madison, WI). Peak positions were determined from the minima in the second derivative of the spectrum.

Domain formation characterization

The organization of the bilayer acyl chains is determined by vibrational infrared spectroscopic measurements. Multilamellar assemblies were prepared of the glycosphingolipid *N*-stearoyl-GalCer by hydrating the lipid in 75% (wt %) H_2O and mixing above T_m (>85°C) before rapid cooling into the gel phase. Once in the gel phase, the temperature was maintained well below the T_m of the lipid with the lowest melting transition (in this work DPPC) to inhibit lipid diffusion. The detected clusters thus represent lipids that are spatially aggregated in the liquid crystalline phase immediately before the gel to liquid crystalline phase transition. To verify that no additional diffusion occurred in the gel, samples were allowed to warm to room temperature over 12 h with the splitting remeasured at −120°C. Samples treated this way exhibited splittings that were identical to those measured immediately. Samples that were left at room temperature for extended periods (>12 h) do begin to show increased correlation field splittings associated with demixing. This behavior over these time periods agrees with previously reported kinetics demixing experiments (32). In the orthorhombic subcell or distorted orthorhombic subcell, a temperature-dependent splitting is observed in the CH_2 (CD_2) methylene deformation modes that correlates directly with the number of hydrocarbon chains forming a lipid microdomain by

$$N = \left[\frac{\pi}{\sqrt{2(1-\Delta\nu/\Delta\nu_0)}} - 1\right]^2, \qquad (1)$$

where N is the number of interacting hydrocarbon chains, $\Delta\nu$ represents the methylene CH_2 or CD_2 mode component splitting in wave numbers, and $\Delta\nu_0$ is a normalization factor equal to the maximum splitting observed in the neat environment of the hydrocarbon chain under investigation (29). For the reference parameter $\Delta\nu_0$, the methylene mode splitting values were obtained at −120°C, the asymptotic maximum region of the splitting component versus temperature profile. For splitting parameters corresponding to larger aggregates (>100 chains), the error in chain number becomes more prob-

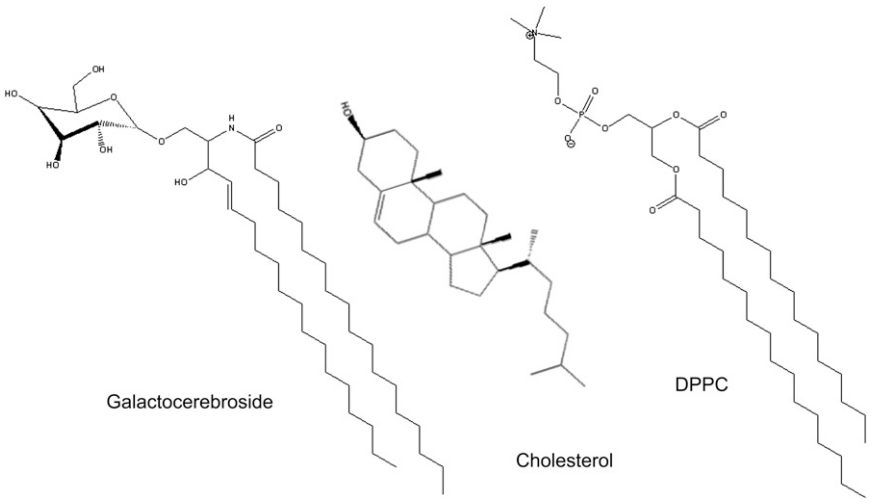

FIGURE 1 Structure of nonhydroxy GalCer, cholesterol, and DPPC.

lematic; however, large splittings are not observed in our data. A reference sample of pure DPPC was measured at appropriate temperatures; DSPC was used as the reference for the microdomains composed of GalCer stearoyl chains. Deuterated chains were ratioed to similarly deuterated reference material whose methylene mode-splitting parameters were determined at low temperatures.

Compressibility measurements

Ultrasonic spectroscopy was performed using a ResoScan acoustic spectrometer (TF Instruments, Monmouth Junction, NJ). The ResoScan spectrometer uses two matched fixed pathlength acoustic transducers to measure the velocity of sound in a sample and a reference channel. For these measurements, ultrapure H_2O was used in the reference chamber. Density measurements for each sample were obtained with a Mettler Toledo DE51 densitometer (Mettler Toledo, Columbus, OH). From precise measurements of the ultrasonic velocity and the density, the total volume adiabatic compressibility (β) of the system can be determined from ultrasonic velocity (u) and the density (ρ) as shown by

$$\beta = \frac{1}{\rho \times u^2}. \tag{2}$$

The apparent volume compressibility of the lipid (β_{lipid}) can be extracted from the ultrasonic velocity increment ([u], the solute concentration-dependent change in ultrasonic velocity), the specific volume of the sample (φ_v), and the adiabatic compressibility of the solvent (β_0) (37,38). A comparison of the relative differences between the sample and reference cells enables high precision measurements of the sample's acoustic properties (37). This differential evaluation relates the adiabatic compressibility of the lipid bilayer assembly to the relative changes in the ultrasonic velocity (u) and the apparent specific volume of the sample (ϕ_v) values, where the ultrasonic velocity increment ([u]) is given by

$$[u] = \frac{(u - u_0)}{c \times u_0}, \tag{3}$$

where c is the concentration of the solute and u and u_0 are the measured ultrasonic velocities of the sample and reference, respectively. The specific volume (φ_v) is determined from the density (ρ) of the sample and referenced as shown by

$$\phi_v = \frac{\left[1 - \frac{(\rho - \rho_0)}{c}\right]}{\rho_0}. \tag{4}$$

The apparent adiabatic compressibility of the lipid is calculated from the velocity number, specific volume of the sample, and adiabatic compressibility of the solvent (β_0, as determined in Eq. 2) by

$$\beta_{\text{lipid}} = \beta_0\left(2 - \frac{[u]}{\phi_v}\right). \tag{5}$$

RESULTS

Fig. 2 *A* displays the low temperature correlation field splitting observed from the 1087 cm^{-1} CD_2 methylene deformation band for a dispersion of pure DPPC-d_{62}. At 20°C the methylene deformation mode at 1087 cm^{-1} remains unsplit and is indicative of a predominantly hexagonal lipid chain phase; but after annealing at −25°C and then cooling to −120°C, a splitting of 8.1 ± 0.2 cm^{-1} for the correlation field components is observed. In Fig. 2 *B*, the CH_2 methylene deformation

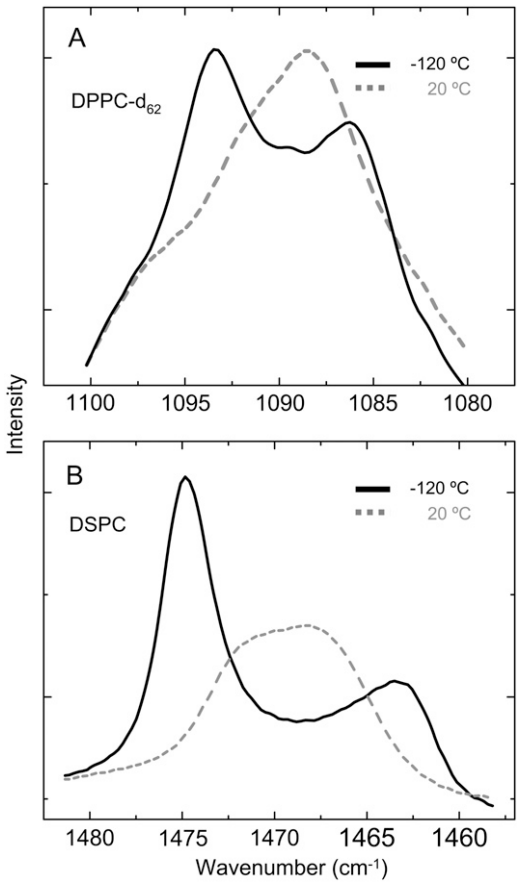

FIGURE 2 Methylene deformation mode is plotted at −120°C (*solid line*) and 20°C (*dashed line*) for CD_2 of DPPC-d_{62} (*A*) and CH_2 of DSPC (*B*). Splitting, proportional to the number of interacting acyl chains, is observed in both cases at low temperature.

is observed to be unsplit at 20°C, whereas a splitting of 12.6 ± 0.4 cm^{-1} is measured at −120°C. It has been shown that the angle of the chain planes with respect to the orthorhombic subcell is determined from

$$\cot(\theta) = \sqrt{\frac{I_a}{I_b}}, \tag{6}$$

where I_a and I_b are intensities of the high- and low-frequency correlation field splitting components, respectively (43). Our data indicate deviations from an ideal orthorhombic chain plane packing arrangement. X-ray diffraction, for example, shows the angle between the chain and an axis of the subcell for orthorhombic n-$C_{23}H_{48}$ to be 42° ± 5° (44). From the intensity ratios of our data, we find this setting angle to be 32° ± 1° for DSPC and 42° ± 3° for DPPC-d_{62}. Cooling to an extreme temperature (−120°C) minimizes the error associated with these deviations.

Fig. 3 *A* displays the absorbance and second derivative spectra in the CH_2 deformation spectral region for a dispersion of pure GalCer at −120°C. The second derivative spectrum was used to accentuate inflections in the line shape

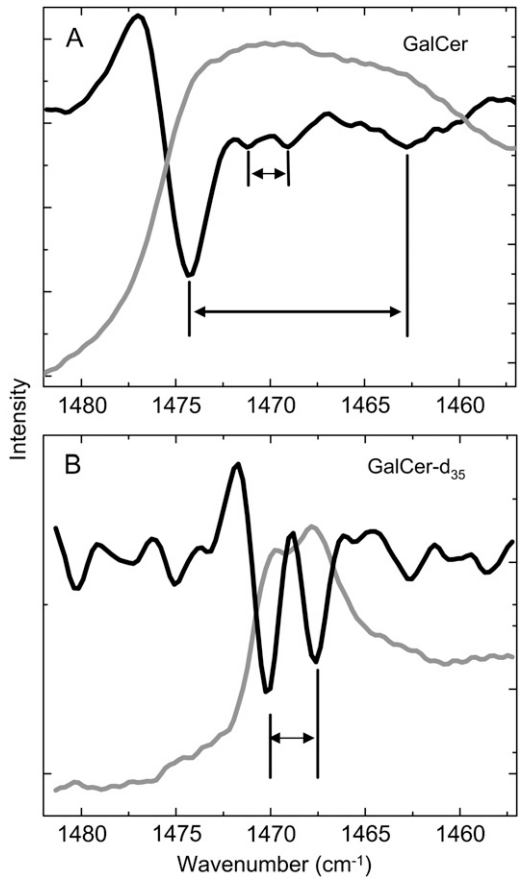

FIGURE 3 Methylene deformation mode of GalCer at −120°C is plotted (*shaded line*) with its second derivative (*solid line*). The second derivative spectra are used to accentuate inflections in the peak line shapes. Two splittings are observed for protonated GalCer (*A*). The inner splitting is shown to arise from the sphingosine chain by examining GalCer-d_{35} with a perdeuterated stearoyl chain (*B*).

for accurate determinations of the peak positions. Two temperature-dependent splittings are observed in the spectrum. The outer splitting was observed initially at −25°C, whereas the inner splitting was not evident until significantly colder temperatures were attained. At −120°C, the outer and inner splittings were determined to be $\Delta\nu_1 = 11.2 \pm 0.2\ cm^{-1}$, and $\Delta\nu_2 = 2.1 \pm 0.1\ cm^{-1}$, respectively. Table 1 records the low temperature correlation field splitting parameters measured for the different lipid systems.

To unambiguously observe and determine the magnitude and origin of the inner splitting components, the experiment was repeated using a GalCer with a deuterated stearoyl chain (GalCer-d_{35}). Fig. 3 *B* clearly demonstrates that the protonated sphingosine chain, in contrast to the stearoyl chain, corresponds to the inner split components observed in Fig. 3 *A*; in the absence of the stearoyl spectral splitting components, $\Delta\nu_2 = 2.6 \pm 0.1\ cm^{-1}$. The slight change in the sphingosine chain component splitting parameters—seen when comparing the protonated and deuterated stearoyl chain GalCer species—may arise from overlapping spectral components in the spectrum of the protonated lipid. Alternatively, differences in the magnitude of the correlation field components may reflect changes in the degree of interchain coupling between the sphingosine and stearoyl chains when both chains represent hydrogenated species. It is important to note that interchain coupling should show larger splitting with both chains isotopically identical and hydrogenated. The increase in splitting when the stearoyl chain is deuterated supports the assertion of the existence of interfering spectral components. Evaluation of the CD_2 deformation correlation field splitting components from GalCer-d35 indicates $\Delta\nu_{1D} = 6.9\ cm^{-1}$.

To correlate the observed splittings with the number of interacting chains for the stearoyl and the sphingosine chains, reference splittings ($\Delta\nu_0$) were acquired from dispersions of DSPC (12.6 cm^{-1}, 8.8 cm^{-1} for DSPC-d_{70} not shown) and DMPC (10.9 cm^{-1}, not shown) determined at −120°C. From Eq. 1, we see that microdomains composed of stearoyl chain aggregates are ~33 chains, whereas sphingosine clusters are ~2–3 chains. A chain number calculation for the deuterated stearoyl chain GalCer indicates only 15 interacting chains. This may indicate some level of interchain coupling in the protonated $\Delta\nu_1$ value; however, the chain coupling that gives rise to the inner splitting, $\Delta\nu_2$, does not seem to be affected, as discussed above. Although DMPC is not a perfect reference for relating the sphingosine chain splitting to cluster size, it does reflect the same number of carbons in the hydrocarbon chain, thus permitting a good approximation. Furthermore, the small splitting observed is near the lower limit of the cluster size calculation. We note that the observation of any correlation field splitting indicates at least two interacting chains.

The CH_2 and CD_2 methylene deformation modes observed from a 1:1 mixture of GalCer and DPPC-d_{62} are shown in Fig. 4. In Fig. 4 *A*, the CH_2 deformation mode exists as a single peak centered at 1469 cm^{-1} at 20°C but is split in a manner similar to that of the pure GalCer dispersion at −120°C. Two separate splitting parameters in the second derivative spectrum are displayed in Fig. 4 *B*. The inner splitting, $2.2 \pm 0.8\ cm^{-1}$, corresponds to the sphingosine chain, whereas the outer splitting of the stearoyl chain is $7.0 \pm 0.1\ cm^{-1}$. This outer splitting for GalCer in the DPPC-d_{62} bilayer matrix corresponds to ~6 chains. In Fig. 4 *C* we note that DPPC-d_{62} also evinces a temperature-dependent change, representative of microdomain formation. From the second derivative spectrum, a $5.9 \pm 0.5\ cm^{-1}$ splitting is determined, corresponding to a microdomain size of ~11 chains. Also evident in the second derivative spectrum of DPPC-d_{62} at −120°C is a substantial contribution at 1089 cm^{-1}, indicating that a portion of the DPPC lipid is in the hexagonal lipid chain phase in addition to the DPPC-d_{62} microdomains.

Addition of 0.33 mol fraction cholesterol to the GalCer/DPPC-d_{62} dispersions dramatically alters the observed spectra, as shown in Fig. 5 for the CH_2 and CD_2 deformation mode regions. In Fig. 5 *A*, although a slight broadening of the CH_2 deformation mode is observed, the second derivative spectrum

TABLE 1 Summary of methylene correlation field splitting parameters at −120°C for both the 1460 cm^{-1} CH_2 and the 1090 cm^{-1} CD_2 deformation components

	CH_2 $\Delta\nu$ (cm^{-1})	CD_2 $\Delta\nu$ (cm^{-1})
DPPC-d_{62}		8.1 ± 0.2
GalCer	*11.2 ± 0.2, †2.1 ± 0.1	
GalCer-d_{35}	†2.6 ± 0.1	*6.9 ± 0.7
DPPC-d_{62} + GalCer	*7.0 ± 0.1, †2.2 ± 0.8	5.9 ± 0.5
DPPC-d_{62} + GalCer + Chol	None apparent	6.0 ± 0.1

*Represents the larger outer splitting associated with the stearoyl chain of GalCer.
†Denotes the smaller inner splitting associated with the sphingosine chain of GalCer.

(Fig. 5 *B*) shows a dominant contribution at 1469 cm^{-1}, representative of a hexagonal lipid chain packing arrangement. The CD_2 splitting of DPPC-d_{62} shows a more subtle change in Fig. 5 *C* with the addition of cholesterol compared to that without cholesterol in Fig. 4. An analysis of the second derivative spectrum (Fig. 5 *D*) indicates a splitting of 6.0 ± 0.1 cm^{-1}, a value within error, that is identical to that observed for the GalCer/DPPC-d_{62} system without cholesterol. Since the intensities of the correlation field components are related to the angle between the packed chain planes (43), the change in infrared absorption splitting component intensities around 1090 cm^{-1} for DPPC-d_{62} at −120°C in Figs. 4 and 5 may indicate a slightly more compact DPPC microdomain in the presence of cholesterol. In Fig. 5 *D*, the peak at 1089 is still evident, indicating the continued existence of mixed hexagonal and orthorhombic phases.

To assess the relative chain ordering in GalCer and its cholesterol complex, the methylene symmetric stretching modes at 2850 and 2090 cm^{-1} were examined. Peak parameters for the symmetric stretching mode were determined from the fit to a single Lorentzian broadened peak with a linear baseline correction. It is well established that as disorder in hydrocarbon chains increases, a corresponding change is observed as an increase in the frequency of the methylene symmetric stretching mode (27). The frequency observed for the CD_2 symmetric stretching modes of DPPC-d_{62} in all lipid systems at both −120°C and 20°C is 2090 ± 0.5 cm^{-1}, consistent with DPPC-d_{62} in the gel phase. Previous results indicate that for DPPC-d_{62} in the more disordered liquid crystalline phase, the peak frequency increases by ~5 cm^{-1} (~3–4 cm^{-1} for DPPC-d_0). The CH_2 symmetric stretching modes of GalCer are observed to be 2850 cm^{-1} at −120°C for both the GalCer/DPPC-d62 and GalCer/Chol/DPPC-d_{62} complexes. At 20°C this frequency is shifted to 2851 cm^{-1} in both systems, indicating a slight increase in disorder.

In addition to chain order, the methylene symmetric stretching mode full width at half-maximum ($\Delta\nu_{1/2}$) provides information about the mobility of the chain moiety, that is, the ability of the molecule to undergo orientational reorganization (45). Table 2 lists the peak frequencies and the values for $\Delta\nu_{1/2}$ for the CD_2 and CH_2 symmetric stretching modes observed for DPPC-d_{62} and for GalCer complexes. The $\Delta\nu_{1/2}$ for DPPC-d_{62} is 12.2 cm^{-1} at −120°C and 14.6 cm^{-1} at 20°C. Mixed with equal mole fractions of GalCer, the $\Delta\nu_{1/2}$ for DPPC-d_{62} is 13.0 cm^{-1} at −120°C and 15.0 cm^{-1} at 20°C. In the DPPC/GalCer/Chol system the $\Delta\nu_{1/2}$ for DPPC-d_{62} is 13.0 and 14.5 cm^{-1} at

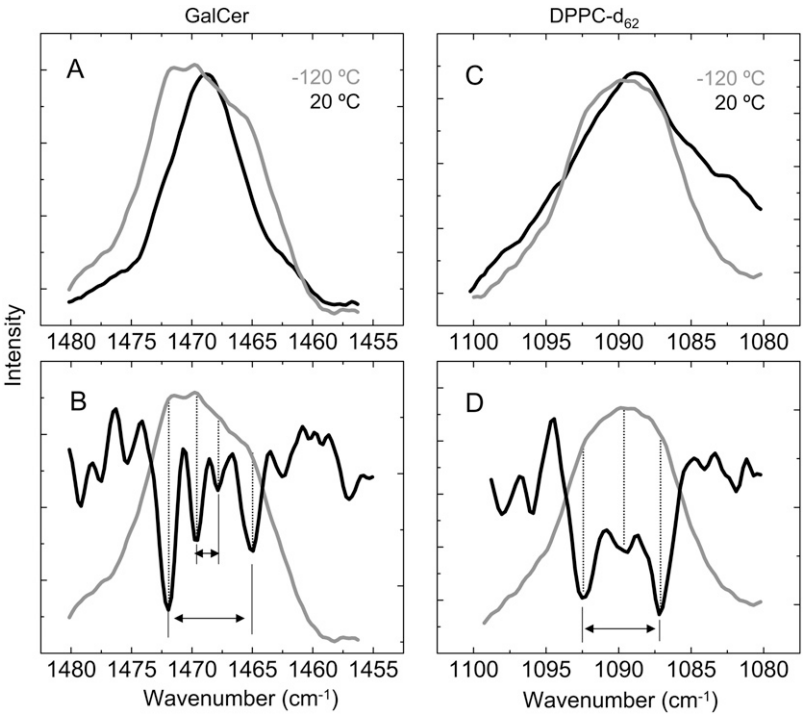

FIGURE 4 Infrared absorption spectra are shown for the methylene deformation regions of a 1:1 mixture of GalCer and DPPC. The CH_2 deformation mode of GalCer is plotted at −120°C and 20°C (*A*). The second derivative spectra (*B*) at −120°C indicates inner and outer peak splitting patterns. The CD_2 deformation mode of DPPC-d_{62} (*C*) also shows a change in line shape at −120°C vs. 20°C. The second derivative spectrum (*D*) at −120°C indicates splitting for the orthorhombic phase as well as the persistence of the hexagonal phase at lower temperature.

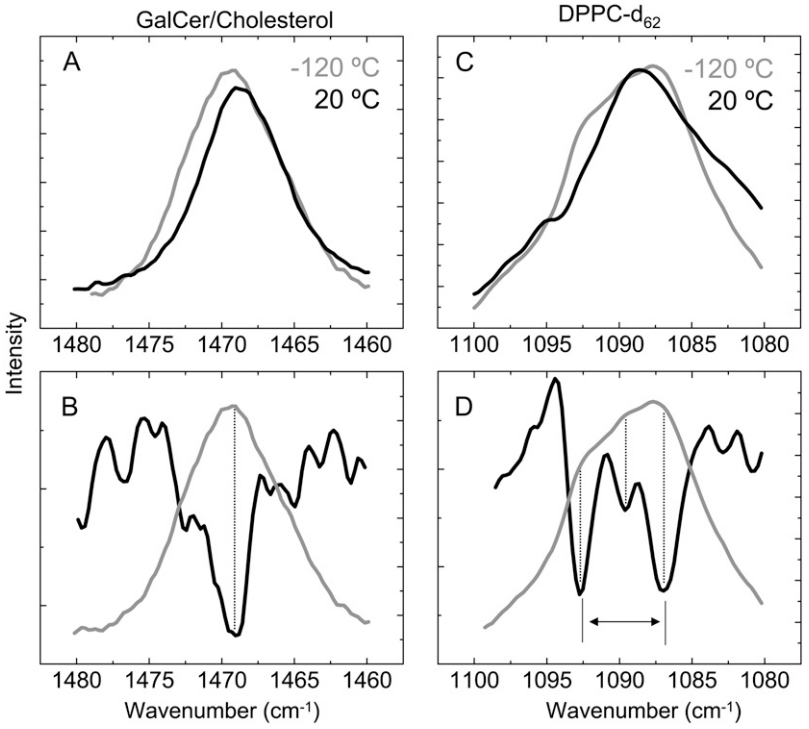

FIGURE 5 Infrared absorption spectra are shown for the methylene deformation regions of a 1:0.33:1 mixture of GalCer, cholesterol, and DPPC. The CH_2 deformation mode of GalCer is plotted at −120°C and 20°C (*A*). The second derivative spectrum (*B*) indicates that the peak exhibits little to no splitting. The CD_2 deformation mode of DPPC-d_{62} is also plotted at −120°C and 20°C (*C*). The second derivative spectrum (*D*) highlights the splitting evident from DPPC.

−120°C and 20°C, respectively. In each system, chain mobility decreases, as expected, at lower temperatures. Analysis of $\Delta\nu_{1/2}$ for the GalCer chains indicates that a larger perturbation is occurring in the mixed systems. When mixed with equal parts DPPC-d_{62}, $\Delta\nu_{1/2}$ for GalCer is 9.1 and 10.1 cm^{-1} at −120°C and 20°C, respectively. The addition of 0.33 mol fraction cholesterol results in a broadening of GalCer CH_2 stretching mode to a halfwidth of 9.8 cm^{-1} at −120°C and to 10.6 cm^{-1} at 20°C. The addition of cholesterol results in a more substantial change in the mobility of the GalCer chains than in the DPPC chains, particularly at −120°C where mobility is strongly inhibited. This is in agreement with the changes observed in the methylene deformation modes, where cholesterol greatly perturbs GalCer but has minimal impact on DPPC.

Ultrasonic velocimetry was performed to determine the total volume adiabatic compressibility of these lipid systems. Velocimetry measurements were performed at 20°C and 63°C, where DPPC exists in the gel and liquid crystalline phases, respectively, in each system. The substantial T_m of GalCer at 85°C places liquid crystalline phase measurements for GalCer beyond the capabilities of the instrument. Table 3 lists the ultrasonic velocity increment ([*u*]), the specific volume (φ_v), and the adiabatic total volume compressibility associated with the lipid (β_{lipid}) determined for our samples. The measurement for pure GalCer was complicated at the higher temperature by the tendency of this lipid to precipitate out of solution and not form ideal vesicle dispersions, thus limiting reproducibility. Upon heating, the specific volume of the samples is seen to increase, as expected with an increase in thermal excitation of the molecules. The changes in the ultrasonic velocity increment represent the combination of specific volume and compressibility changes. For DPPC, the specific volume increases by a factor of 3; however, the ultrasonic velocity increment dramatically decreases.

Calculation of the compressibility of the DPPC shows little change, indicating that ultrasonic velocity decreases because of decreased density of the sample. In the 1:1 GalCer/DPPC sample a much more modest increase is observed in φ_v. The addition of GalCer results in the formation of microdomains,

TABLE 2 Symmetric methylene stretching mode frequencies and bandwidths for DPPC-d_{62} and GalCer assemblies at −120°C and 20°C

	DPPC-d_{62}				GalCer			
	−120°C		20°C		−120°C		20°C	
	ν (cm^{-1})	$\Delta\nu_{1/2}$	ν (cm^{-1})	$\Delta\nu_{1/2}$	ν (cm^{-1})	$\Delta\nu_{1/2}$	ν (cm^{-1})	$\Delta\nu_{1/2}$
DPPC	2090.3 ± 0.1	12.2 ± 0.1	2089.3 ± 0.4	14.6 ± 0.5	-	-	-	-
DPPC + GalCer	2090.0 ± 0.1	13.0 ± 0.1	2089.5 ± 0.2	15.0 ± 0.8	2849.7 ± 0.3	9.1 ± 0.2	2851.0 ± 0.2	10.1 ± 0.6
DPPC + GalCer + Chol	2089.7 ± 0.1	13.0 ± 0.1	2089.4 ± 0.1	14.5 ± 0.5	2850.1 ± 0.2	9.8 ± 0.5	2851.4 ± 0.2	10.6 ± 0.5

TABLE 3 Ultrasonic velocimetry characteristics, ultrasonic velocity increment ([u]), specific volume (ϕ_v), and adiabatic compressibility (β_{lipid}) determined at 20°C and 63°C

	[u] ($\times 10^{-2}$ mL/g)		φ_v ($\times 10^{-2}$ mL/g)		β_{lipid} ($\times 10^{-11}$ Pa^{-1})	
	20°C	63°C	20°C	63°C	20°C	63°C
DPPC	13.56 ± 0.14	−13.09 ± 0.13	93.06 ± 0.16	271.4 ± 1.7	82 ± 2.5	84 ± 2.5
DPPC + GalCer	23.99 ± 0.24	26.3 ± 0.03	92.70 ± 0.16	111.8 ± 0.17	77 ± 2.3	81 ± 2.4
DPPC + GalCer + Chol	17.47 ± 0.17	−16.96 ± 0.17	92.76 ± 0.16	100.9 ± 0.14	80 ± 2.4	89 ± 2.7
GalCer	1.71 ± 0.020	-	96.67 ± 0.14	-	88 ± 3.8	-

The reported error represents the experimental uncertainty of the measurement, as replicated measurements exhibited greater precision.

as discussed above, changing the intermolecular interactions. At elevated temperatures, the significantly different and more modest change in [u] and φ_v suggests that these intermolecular interactions may persist. The addition of cholesterol shows a similarly modest change in φ_v to that of the 1:1 dispersion; however the change in [u] corresponds to a more significant change in compressibility. From the infrared spectroscopic measurements, cholesterol significantly perturbs the GalCer domains, perhaps increasing the compressibility of these aggregates. The total volume adiabatic compressibility, calculated for each sample, graphed in Fig. 6, decreases for the GalCer/DPPC system relative to the pure lipids. However, the addition of cholesterol to the system results in an increase in adiabatic compressibility. This trend holds at both temperatures measured. It is worth noting that the increase in compressibility with the addition of cholesterol is significantly greater at 63°C.

DISCUSSION

We present a new (to our knowledge) approach to structurally characterizing model lipid microdomain complexes using both vibrational infrared spectroscopy and ultrasonic velocimetry. One challenge associated in describing microdomain complexes is the rapid diffusion of lipids in the liquid crystalline phase. Our approach is to prepare our assemblies in the liquid crystalline phase and then rapidly cool the dispersions to induce the gel phase where lateral diffusion is dramatically inhibited. This method provides a representation of the lipid distributions and organization in the liquid crystalline phase before becoming immobilized in the gel phase. Our findings point to lipid microdomains which are nanometer in scale, in contrast to the micron-sized domains more commonly found in phase-separated systems (1,11,12).

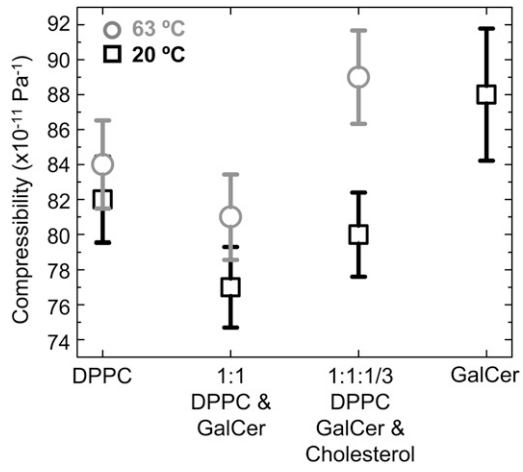

FIGURE 6 Compressibility of the different lipid dispersions is plotted at 20°C (*solid squares*) and at 63°C (*shaded circles*). At 63°C DPPC is in the liquid crystalline phase, whereas GalCer remains in gel phase at both temperatures.

The number of hydrocarbon chains in the clusters stated in our results reflects a lower bound for the actual cluster size of the lipid microdomains. Modeling (29) indicates that a compact domain geometry (as calculated in Eq. 1) requires fewer hydrocarbon chains than does an irregularly shaped domain. The 5.9 cm^{-1} splitting observed for DPPC-d_{62} in the presence of GalCer corresponds to a compact microdomain of 11 chains, or extrapolating from the model of Snyder et al. for an irregular microdomain arrangement (29), this same methylene mode splitting parameter may represent ~20 chains. The number of interacting lipid chains calculated from the infrared CH_2 deformation mode splitting pattern agrees with cluster determinations for lipids calculated from calorimetry (46) and fluorescence measurements (47). For a compact domain assuming a square geometry, these 11 chains may correspond to a cluster of ~15 nm in width. This cluster size is in agreement with that for lipid aggregates in intact membranes as determined by FRET (16) and ultrafast freezing with antibody capture (48). In the infrared measurements, no exogenous probe is introduced, thus eliminating the possibility of undesired molecular perturbations or interactions. Consequently, the small domains detected here may be a fundamental microcluster size for lipids in intact membranes, further suggesting that larger domains may result from cluster aggregation.

Normal coordinate analyses have shown that the deformation mode splitting parameters arise explicitly from the interaction of CH_2 oscillators arranged in an orthorhombic subcell (43). Significant deviation from an orthorhombic chain packing arrangement reduces chain-chain interactions. Lipid acyl chains in a hexagonal packing orientation do not give rise to correlated field splitting interactions. The observation of two distinct splittings, and confirmation by deuteration of the

stearoyl chain in GalCer, provides direct evidence of an additional higher organization within the lipid bilayers. The sphingosine chains specifically cluster into aggregates of two to three lipids, connected within a larger interconnected orthorhombic lattice of stearoyl-GalCer chains. The stronger van der Waals interactions inherent in the stearoyl chains promote stearoyl chain coupling, leaving the accompanying sphingosine chain to interact with a nearest chain. The cluster size for the GalCer lipid is thus best represented here by a larger, interconnected stearoyl chain arrangement. The double bond in the sphingosine chain allows chain disordering, which apparently inhibits orthorhombic packing, as reflected in the observation of only small orthorhombic, sphingosine pockets within the interconnected stearoyl lattice of GalCer aggregates. From the observed splittings, a new picture arises regarding the organization of these lipids within the bilayer.

Glycosphingolipids, such as GalCer, generally occur in low concentrations in both plant and animal tissues (49); however, in specialized tissue, such as the microvilli of the intestine and the myelin sheath, these sphingolipids represent a substantial portion of the total membrane lipid composition (50–52). Indeed, the carbohydrate and fatty acid moieties of these lipids are reported to play key roles in surface phenomena such as cell recognition and adhesion (2). The measurements we present suggest that specific interactions between the acyl chains of GalCer or other matrix lipids may drive the higher organization of lipid species within the bilayer that may be involved in regulating intact membrane function.

The textbook lipid raft is a sphingolipid/cholesterol-enriched microdomain. The addition of cholesterol to our model domain disrupts the lipid chain orthorhombic subcell, induced at low temperature, complicating quantitation of the raft size. From our results two significant possibilities exist: either GalCer microdomains are disrupted by cholesterol, which promotes a mixed GalCer/DPPC-d_{62}/Chol phase, or, alternatively, the GalCer domains persist but the intercalation of cholesterol inhibits the chain planes from forming orthorhombic subcells. Our method does not permit a distinction between these possibilities. The results indicate that cholesterol shows significant preference for the glycosphingolipid in comparison to the desaturated phosphatidylcholine species. This preference is somewhat surprising in light of a recent model purporting that larger headgroups provide an umbrella to minimize exposure of the largely hydrophobic cholesterol to the aqueous phase (53).

Single sugars are reported to be comparable in size to phosphatidylethanolamine headgroups (54); however, phosphatidylcholine headgroups have been reported to be more efficient at shielding hydrophobic moieties than is the phosphatidylethanolamine headgroup (53). Under the umbrella model, one would expect to observe cholesterol preferentially disrupting the DPPC aggregates in the bilayer matrix. At the low concentration of cholesterol used in these experiments, a clear preference of cholesterol was observed for the GalCer species. Although the umbrella effect may dominate at high cholesterol content, 1:1 or higher molar ratios, low cholesterol contents lead to preferential interactions with the sphingolipid component. This is in agreement with previous studies demonstrating that cholesterol interacts preferentially with the sphingolipid backbone (55–57).

The role of cholesterol in microdomain behavior is elucidated by the combined acoustic and infrared measurements. The 1:1 mixture of GalCer and DPPC shows a decreased compressibility relative to that for the pure components. This can be interpreted to result from the ensemble packing of larger domains. That is, larger microdomains pack as groups less effectively than, for example, the individual lipids pack into a single cluster. Upon the addition of cholesterol, we observe a modest increase in the gel phase total compressibility of the system and a much more substantial change at higher temperature. Within the model of large domains packing less effectively, this indicates a disruption of the GalCer domains. Others have demonstrated, using AFM and supported bilayers, that cholesterol increases GalCer and phospholipid miscibility, which would inhibit domain structures (21). Examination of the CH_2 symmetric stretching mode bandwidths supports a more mobile GalCer species as this $\Delta\nu_{1/2}$ increases at $-120°C$ and, though more modestly, at room temperature in comparison to $\Delta\nu_{1/2}$ values for DPPC, which are unaffected.

A principal challenge for characterizing lipid rafts and other microdomains is to understand the behavior of these systems in the highly dynamic liquid crystalline phase. In the experiments presented here, the lipid assemblies are rapidly cooled to capture the distribution of lipids representative of the liquid crystalline phase. The reduced diffusion in the gel phase permits characterization of the system without a further potential phase separation. The infrared methylene deformation mode splitting patterns used to characterize microdomain sizes do not occur in the liquid crystalline phase. This splitting is associated with the packing of the lipids within an orthorhombic subcell, which is only obtained at low temperatures. Because of the rapid freezing of the dispersions from the liquid crystalline phase, the absence of this splitting at higher temperatures provides no bearing on the presence or absence of domains, but implies the existence of hexagonal chain packing arrangements.

It is interesting to note, however, that the qualitative trends observed for compressibility of the rapidly cooled assemblies is maintained upon heating the system into the liquid crystalline phase region of DPPC. Specifically, the 1:1 GalCer/DPPC assembly suggests a trend toward a reduced compressibility at both temperatures relative to the pure components, with the addition of cholesterol suggesting increases in the total compressibility of the system. Furthermore, both systems show similar changes in specific volume with elevated temperature, which are significantly different from the pure DPPC lipid matrix. It is also worth noting that the aggregate size, determined from the correlation field splitting parameters, is consistent between the two types of aggregates. This further suggests that 1), the lipid aggregates may exist as equilibrium

structures, since nonequilibrium domains would be expected to have greater dispersions in their domain sizes; and 2), molecular associations exist in the liquid crystalline phase that are similar to those determined by infrared measurements for the gel phase. These generic clusters may provide interesting targets for probing intact membranes.

The changes in the total compressibility of the system provide further insight into the role of lipids in modulating membrane activity. Langmuir balance measurements indicate decreased lateral compressibility when cholesterol is added to mixed sphingomyelin species, which contains assorted different acyl chains (55). If the differences in acyl chains have a negligible impact, the increase in total volume compressibility observed in our measurements suggests that a transbilayer compressibility component also exists. Additionally, these experiments suggest that the compressibility of the membrane complex can be tuned by varying the microdomain components. Future experiments involving more sophisticated systems including transmembrane proteins will likely prove enlightening.

CONCLUSIONS

These results provide to our knowledge a new platform for studying the interactions that lead to the formation of microdomains. The magnitude of the acyl chain methylene mode infrared splitting parameters determined at low temperature permits an estimate of microdomain sizes. Since this splitting parameter is sensitive to the lipid acyl chain packing environment, investigations into specific intermolecular interactions are feasible. By appropriately deuterating various chain components, a detailed perturbation due to additional molecules to a domain structure can be assessed since separate chain species can be monitored. Additionally, ultrasonic velocimetry permits characterization of the mechanical compressibility characteristics of these model systems. The adiabatic compressibility parameter provides insight into the characteristics of the lipid matrix that in part regulate the behavior of integral membrane components.

The authors thank Dr. Theodor Funck and TF Instruments for helpful discussion and the temporary use of the Resoscan acoustic spectrometer. The authors also thank Dr. Abdellah Menikh for initial discussions.

Z.D.S. acknowledges support from a National Research Council/National Institute of Standards and Technology postdoctoral fellowship. This work was funded through the National Institute of Diabetes and Digestive and Kidney Diseases, National Institutes of Health intramural research program.

REFERENCES

1. Edidin, M. 2003. The state of lipid rafts: from model membranes to cells. *Annu. Rev. Biophys. Biomol. Struct.* 32:257–283.
2. Brown, D. A., and E. London. 1998. Functions of lipid rafts in biological membranes. *Annu. Rev. Cell Dev. Biol.* 14:111–136.
3. Vereb, G., J. Szollosi, J. Matko, P. Nagy, T. Farkas, L. Vigh, L. Matyus, T. A. Waldmann, and S. Damjanovich. 2003. Dynamic, yet structured: the cell membrane three decades after the Singer-Nicolson model. *Proc. Natl. Acad. Sci. USA.* 100:8053–8058.
4. Jacobson, K., O. G. Mouritsen, and R. G. W. Anderson. 2007. Lipid rafts: at a crossroad between cell biology and physics. *Nat. Cell Biol.* 9:7–14.
5. Varma, R., and S. Mayor. 1998. GPI-anchored proteins are organized in submicron domains at the cell surface. *Nature.* 394:798–801.
6. Schroeder, R. J., S. N. Ahmed, Y. Z. Zhu, E. London, and D. A. Brown. 1998. Cholesterol and sphingolipid enhance the Triton X-100 insolubility of glycosylphosphatidylinositol-anchored proteins by promoting the formation of detergent-insoluble ordered membrane domains. *J. Biol. Chem.* 273:1150–1157.
7. Simons, K., and E. Ikonen. 1997. Functional rafts in cell membranes. *Nature.* 387:569–572.
8. Brown, D. A., and J. K. Rose. 1992. Sorting of GPI-anchored proteins to glycolipid-enriched membrane subdomains during transport to the apical cell surface. *Cell.* 68:533–544.
9. Simons, K., and A. Wandingerness. 1990. Polarized sorting in epithelia. *Cell.* 62:207–210.
10. Simons, K., and G. Vanmeer. 1988. Lipid sorting in epithelial cells. *Biochemistry.* 27:6197–6202.
11. London, E. 2005. How principles of domain formation in model membranes may explain ambiguities concerning lipid raft formation in cells. *Biochim. Biophys. Acta.* 1746:203–220.
12. Silvius, J. R. 2005. Partitioning of membrane molecules between raft and non-raft domains: insights from model-membrane studies. *Biochim. Biophys. Acta.* 1746:193–202.
13. Veatch, S. L., and S. L. Keller. 2003. Separation of liquid phases in giant vesicles of ternary mixtures of phospholipids and cholesterol. *Biophys. J.* 85:3074–3083.
14. Lagerholm, B. C., G. E. Weinreb, K. Jacobson, and N. L. Thompson. 2005. Detecting microdomains in intact cell membranes. *Annu. Rev. Phys. Chem.* 56:309–336.
15. Miersch, S., and B. Mutus. 2007. Membrane lipid domains: techniques for visualization and characterization. *Curr. Anal. Chem.* 3:81–92.
16. Sengupta, P., D. Holowka, and B. Baird. 2007. Fluorescence resonance energy transfer between lipid probes detects nanoscopic heterogeneity in the plasma membrane of live cells. *Biophys. J.* 92:3564–3574.
17. Veatch, S. L., S. S. W. Leung, R. E. W. Hancock, and J. L. Thewalt. 2007. Fluorescent probes alter miscibility phase boundaries in ternary vesicles. *J. Phys. Chem. B.* 111:502–504.
18. Shaw, J. E., R. F. Epand, R. M. Epand, Z. G. Li, R. Bittman, and C. M. Yip. 2006. Correlated fluorescence-atomic force microscopy of membrane domains: structure of fluorescence probes determines lipid localization. *Biophys. J.* 90:2170–2178.
19. Wang, T. Y., and J. R. Silvius. 2000. Different sphingolipids show differential partitioning into sphingolipid/cholesterol-rich domains in lipid bilayers. *Biophys. J.* 79:1478–1489.
20. Zhang, L., and S. Granick. 2005. Lipid diffusion compared in outer and inner leaflets of planar supported bilayers. *J. Chem. Phys.* 123:211104.
21. Blanchette, C. D., W.-C. Lin, T. V. Ratto, and M. L. Longo. 2006. Galactosylceramide domain microstructure: impact of cholesterol and nucleation/growth conditions. *Biophys. J.* 90:4466–4478.
22. Kraft, M. L., P. K. Weber, M. L. Longo, I. D. Hutcheon, and S. G. Boxer. 2006. Phase separation of lipid membranes analyzed with high-resolution secondary ion mass spectrometry. *Science.* 313:1948–1951.
23. Harroun, T. A., W. T. Heller, T. M. Weiss, L. Yang, and H. W. Huang. 1999. Experimental evidence for hydrophobic matching and membrane-mediated interactions in lipid bilayers containing gramicidin. *Biophys. J.* 76:937–945.
24. Lundbaek, J., and O. Andersen. 1994. Lysophospholipids modulate channel function by altering the mechanical properties of lipid bilayers. *J. Gen. Physiol.* 104:645–673.
25. Hwang, T.-C., R. E. Koeppe, and O. S. Andersen. 2003. Genistein can modulate channel function by a phosphorylation-independent mechanism:

importance of hydrophobic mismatch and bilayer mechanics. *Biochemistry*. 42:13646–13658.

26. Jensen, M. O., and O. G. Mouritsen. 2004. Lipids do influence protein function—the hydrophobic matching hypothesis revisited. *Biochim. Biophys. Acta*. 1666:205–226.
27. Levin, I. W. 1984. Vibrational spectroscopy of membrane assemblies. *In* Advances in Infrared and Raman Spectroscopy. R. G. H. Clark and R. E. Hester, editors. Wiley Heyden, New York. 1–48.
28. Jackson, M., D. J. Moore, H. H. Mantsch, and R. Mendelsohn. 2002. Vibrational spectroscopy of membranes. *In* Handbook of Vibrational Spectroscopy. J. M. Chalmers and P. R. Griffiths, editors. John Wiley & Sons, Chichester, UK. 3508–3518.
29. Snyder, R. G., M. C. Goh, V. J. P. Srivatsavoy, H. L. Strauss, and D. L. Dorset. 1992. Measurement of the growth-kinetics of microdomains in binary *N*-alkane solid-solutions by infrared-spectroscopy. *J. Phys. Chem.* 96:10008–10019.
30. Mendelsohn, R., G. L. Liang, H. L. Strauss, and R. G. Snyder. 1995. IR spectroscopic determination of gel state miscibility in long-chain phosphatidylcholine mixtures. *Biophys. J*. 69:1987–1998.
31. Snyder, R. G., G. L. Liang, H. L. Strauss, and R. Mendelsohn. 1996. IR spectroscopic study of the structure and phase behavior of long-chain diacylphosphatidylcholines in the gel state. *Biophys. J*. 71:3186–3198.
32. Moore, D. J., R. G. Snyder, M. E. Rerek, and R. Mendelsohn. 2006. Kinetics of membrane raft formation: fatty acid domains in stratum corneum lipid models. *J. Phys. Chem. B*. 110:2378–2386.
33. Kharakoz, D. P., A. Colotto, K. Lohner, and P. Laggner. 1993. Fluid-gel interphase line tension and density fluctuations in dipalmitoylphosphatidylcholine multilamellar vesicles: an ultrasonic study. *J. Phys. Chem.* 97:9844–9851.
34. Mitchell, D. C., M. Straume, and B. J. Litman. 1992. Role of *sn*-1-saturated,*sn*-2-polyunsaturated phospholipids in control of membrane receptor conformational equilibrium: effects of cholesterol and acyl chain unsaturation on the metarhodopsin I in equilibrium with metarhodopsin II equilibrium. *Biochemistry*. 31:662–670.
35. Niu, S. L., D. C. Mitchell, and B. J. Litman. 2001. Optimization of receptor-G protein coupling by bilayer lipid composition II: Formation of metarhodopsin II-transducin complex. *J. Biol. Chem.* 276:42807–42811.
36. Mitchell, D. C., S. L. Niu, and B. J. Litman. 2001. Optimization of receptor-G protein coupling by bilayer lipid composition I: Kinetics of rhodopsin-transducin binding. *J. Biol. Chem.* 276:42801–42806.
37. Sarvazyan, A. P. 1991. Ultrasonic velocimetry of biological compounds. *Annu. Rev. Biophys. Biophys. Chem.* 20:321–342.
38. Hianik, T., M. Haburcak, K. Lohner, E. Prenner, F. Paltauf, and A. Hermetter. 1998. Compressibility and density of lipid bilayers composed of polyunsaturated phospholipids and cholesterol. *Colloids Surf. A Physicochem. Eng. Asp*. 139:189–197.
39. Hianik, T., P. Rybar, G. M. Kostner, and A. Hermetter. 1997. Molecular acoustic as a new tool for the study of biophysical properties of lipoproteins. *Biophys. Chem.* 67:221–228.
40. Taulier, N., and T. V. Chalikian. 2002. Compressibility of protein transitions. *Biochim. Biophys. Acta*. 1595:48–70.
41. Taulier, N., I. V. Beletskaya, and T. V. Chalikian. 2005. Compressibility changes accompanying conformational transitions of apomyoglobin. *Biopolymers*. 79:218–229.
42. Taylor, T. M., P. M. Davidson, B. D. Bruce, and J. Weiss. 2005. Ultrasonic spectroscopy and differential scanning calorimetry of liposomal-encapsulated nisin. *J. Agric. Food Chem.* 53:8722–8728.
43. Snyder, R. G. 1961. Vibrational spectra of crystalline *n*-paraffins. II. Intermolecular effects. *J. Mol. Spectrosc*. 7:116–144.
44. Smith, A. E. 1953. The crystal structure of the normal paraffin hydrocarbons. *J. Chem. Phys*. 21:2229–2231.
45. Rothschild, W. 1984. Dynamics of Molecular Liquids. John Wiley & Sons, New York.
46. Anderson, T. G., and H. M. McConnell. 2002. A thermodynamic model for extended complexes of cholesterol and phospholipid. *Biophys. J*. 83:2039–2052.
47. Radhakrishnan, A., T. G. Anderson, and H. M. McConnell. 2000. Condensed complexes, rafts, and the chemical activity of cholesterol in membranes. *Proc. Natl. Acad. Sci. USA*. 97:12422–12427.
48. Rock, P., M. Allietta, W. W. Young, T. E. Thompson, and T. W. Tillack. 1990. Organization of glycosphingolipids in phosphatidylcholine bilayers—use of antibody molecules and Fab fragments as morphological markers. *Biochemistry*. 29:8484–8490.
49. Koshy, K. M., and J. M. Boggs. 1983. Partial synthesis and physical properties of cerebroside sulfate containing palmitic acid or alpha-hydroxy palmitic acid. *Chem. Phys. Lipids*. 34:41–53.
50. Morell, P., and W. T. Norton. 1980. Myelin. *Sci. Am*. 242:88–117.
51. Breimer, M. E. 1975. Distribution of molecular species of sphingomyelins in different parts of bovine digestive tract. *J. Lipid Res*. 16: 189–194.
52. Breimer, M. E., K. A. Karlsson, and B. E. Samuelsson. 1974. The distribution of molecular species of monoglycosylceramides (cerebrosides) in different parts of bovine digestive tract. *Biochim. Biophys. Acta*. 348:232–240.
53. Ali, M. R., K. H. Cheng, and J. Huang. 2006. Ceramide drives cholesterol out of the ordered lipid bilayer phase into the crystal phase in 1-palmitoyl-2-oleoyl-*sn*-glycero-3-phosphocholine/cholesterol/ceramide ternary mixtures. *Biochemistry*. 45:12629–12638.
54. Hinz, H. J., L. Six, K. P. Ruess, and M. Lieflaender. 1985. Head-group contributions to bilayer stability: monolayer and calorimetric studies on synthetic, stereochemically uniform glucolipids. *Biochemistry*. 24:806–813.
55. Li, X.-M., M. M. Momsen, J. M. Smaby, H. L. Brockman, and R. E. Brown. 2001. Cholesterol decreases the interfacial elasticity and detergent solubility of sphingomyelins. *Biochemistry*. 40:5954–5963.
56. Ramstedt, B., and J. P. Slotte. 1999. Interaction of cholesterol with sphingomyelins and acyl-chain-matched phosphatidylcholines: a comparative study of the effect of the chain length. *Biophys. J*. 76:908–915.
57. McQuaw, C. M., L. L. Zheng, A. G. Ewing, and N. Winograd. 2007. Localization of sphingomyelin in cholesterol domains by imaging mass spectrometry. *Langmuir*. 23:5645–5650.